Article

Al-ZSM-5 Nanocrystal Catalysts Grown from Silicalite-1 Seeds for Methane Conversion

Hyun Su Kim [1,2], Su Kyung Kang [1], Haoxiang Zhang [1], Elsa Tsegay Tikue [1,2], Jin Hyung Lee [3,*] and Pyung Soo Lee [1,2,*]

1   Department of Chemical Engineering and Material Science, Chung-Ang University, 84, Heukseok-ro, Seoul 06974, Korea; hyunsu0718@cau.ac.kr (H.S.K.); hllysk91@cau.ac.kr (S.K.K.); hansel@cau.ac.kr (H.Z.); et2019220258@cau.ac.kr (E.T.T.)
2   Department of Intelligent Energy and Industry, Chung-Ang University, 84, Heuksek-ro, Seoul 06974, Korea
3   Convergence R&D Division, Korea Institute of Ceramic Engineering and Technology (KICET), Cheongju 28160, Chungbuk, Korea
*   Correspondence: leejinh1@kicet.re.kr (J.H.L.); leeps@cau.ac.kr (P.S.L.); Tel.: +82-43-913-1502 (J.H.L.); +82-2-820-5939 (P.S.L.)

Abstract: This study evaluated Al-ZSM-5 nanocrystals grown from silicalite-1 seed crystals as catalysts for the methane dehydroaromatization (MDA) reaction. Silicalite-1 seed crystals sized between 30 and 40 nm were used to grow Al-ZSM-5 under various synthesis conditions. The size of Al-ZSM-5 was significantly affected by the Si/Al ratio (SAR), synthesis time, and silica nutrients/seed crystal ratio (NSR). Larger crystals were obtained with an increased SAR in the synthesis sols. Gradual growth of Al-ZSM-5 occurred with synthesis time, although the growth in crystal size ceased at 5 h of synthesis at 120 °C, indicating the rapid growth of Al-ZSM-5 aided by the silicalite-1 seeds. Precise tuning of Al-ZSM-5 size was possible by changing the nutrient/silicalite-1 seed ratio; a higher NSR led to larger crystals. Two representative Al-ZSM-5 crystals with SARs of 35 and 140 were prepared for catalyst testing, and the crystal sizes were tailored to <100 nm by controlling NSR. The MDA reaction was conducted in the presence of the prepared Al-ZSM-5. The catalyst size exhibited distinct differences in catalyst stability, while the SAR of catalysts did not produce noticeable changes in the catalyst stability of the Al-ZSM-5 crystals and commercial zeolites in this reaction system.

Keywords: silicalite-1; Al-ZSM-5 zeolites; methane dehydroaromatization; diffusion; nanocrystal

1. Introduction

Zeolites are microporous inorganic materials that are characterized by their unique shape selectivity and interconnected acidic pore channels [1,2]. For improved access to abundant natural gas resources, zeolites have been tested as catalysts to convert methane into syngas, liquid chemicals, and fuels via catalytic acid reactions [3]. The methane dehydroaromatization (MDA) reaction in the presence of the ZSM-5 catalyst is an efficient means of converting methane into benzene and hydrogen [4]. The facile isomorphous substitution [5–8], aromatic selective pores [9–11], and strong Brønsted acid sites [12] of ZSM-5 improve its conversion kinetics. However, commercialization of the MDA reaction over ZSM-5 is yet to occur due to its rapid catalyst deactivation, low equilibrium conversion, and complex reaction pathways [13]. There has been extensive research directed at addressing these issues through catalyst design [10,12], reaction system engineering [14,15], and elucidation of the reaction mechanism [16,17].

Based on the well-known bifunctional mechanisms of the MDA reaction, methane activates on the surface of metal oxides and transforms into C_2-based molecules following the induction period [17]. These C_2 molecules convert into aromatics in the acid pore channels of ZSM-5 [18]. As the MDA reaction progresses, graphitic coke is deposited on the metal oxide surface and Brønsted acid sites of the zeolite due to excessive aromatization;

this eventually deactivates the catalyst [13,16]. In this reaction, the Brønsted acid sites in ZSM-5 offer anchoring locations for metal ions while preparing the catalysts and play the role of acid catalysts for the cyclization of intermediates to aromatics during the reaction [19,20]. The morphology of ZSM-5 determines the dispersion of metals in zeolite pores, the diffusion of methane, and the reaction products along the micropores [11,12]. Thus, the rational design of ZSM-5 is a critical for the MDA reaction. To date, preliminary studies have investigated the correlation between MDA reaction kinetics and the properties of ZSM-5.

There are reports of various synthesis techniques to tailor the morphology of zeolites. Soft templating methods, involving the use of specially designed structure-directing agents (SDAs) [21–24], have been used to tailor zeolite morphology. In the hard templating method, mesoporous zeolites crystallize inside rigid mesoporous templates such as amorphous carbon and ordered carbon [10,25]. Post-treatment methods such as desilication [26] and dealumination [27] have also been shown to produce mesoporous structures. These synthesis approaches yield products with diverse nanoscopic morphologies such as pillared structures [21], house-of-card structures [23], nanosheets [22], and ordered/disordered mesoporous structures [23,25]. The pillared MFI structure developed by Choi et al. [21] demonstrated an improved catalytic lifetime for the methanol-to-gasoline reaction. Wu et al. [11] reported on the correlation between the diffusion length and the performance of crystalline catalysts for the MDA reaction.

To some extent, zeolite morphology may be tailored by controlling synthesis parameters such as reaction temperature, synthesis time, and gel composition without using specially designed organic and inorganic templates [28,29]. However, zeolite nucleation is very difficult to control due to its complexity; this inhibits the tuning of zeolite morphology [30,31]. The seeded growth approach is where seed crystals composed of similar building units of the targeted zeolite are added to the synthesis sol [29,32,33]. This approach has been investigated as an alternative means of customizing zeolite morphology. In this method, seed crystals act as the nuclei for zeolite growth, circumventing the uncontrollable nucleation step. This means that zeolite crystal morphology may be precisely controlled by regulating zeolite growth rate and direction. Zeolite crystals with various surface morphologies have been prepared using the seed growth method [34,35]. This method offers several advantages such as short crystallization time, SDA-free growth, and reduced impurities [29,32].

In this study, we prepared Al-ZSM-5 crystals to use in the MDA reaction. To explore the effect of zeolite diffusion length on catalyst stability during the MDA reaction, monodisperse Al-ZSM-5 with a crystal size < 100 nm was synthesized by growing Al-ZSM-5 on silicalite-1 seeds between 30 and 40 nm. Preparation of the monodispersed Al-ZSM-5 nanocrystals via seeded growth on silicalite-1 as catalysts intended for MDA reaction has not been investigated. The Al-ZSM-5 crystals that were grown consisted of a short activation channel of 60 nm on the outer layer and a core of silicatlite-1 seed. This zeolite configuration contributes to suppressing catalyst deactivation by shortening the diffusion length of reactants and is expected to facilitate the loading of bulky Mo metal oxides into micropores of zeolites during preparation of MDA catalysts. In this study, Al-ZSM-5 was first grown on silicalite-1 seeds. Then, zeolite growth kinetics and crystal design parameters, such as the Si/Al ratio (SAR), reaction temperature, crystallization time, and silicalite-1/silica nutrient ratio were analyzed. This led to the preparation of two nanocrystalline Al-ZSM-5 crystals that were <100 nm, for the MDA reaction. The physico-chemical properties of these crystals were characterized by field emission scanning electron microscopy (FE-SEM), energy dispersive spectroscopy (EDS), X-ray powder diffraction (XRD), and nitrogen gas isotherms. The MDA reaction was conducted in the presence of the Al-ZSM-5 catalyst, and the corresponding stability of the catalyst was evaluated and compared with micron-sized commercial Al-ZSM-5 crystals.

2. Materials and Method

2.1. Materials

Tetraethyl orthosilicate (TEOS, 98%), silicic acid (99.9%), tetrapropylammonium hydroxide (TPAOH, 1M), and ammonium heptamolybdate ($(NH_4)_6Mo_7O_{24}\cdot4H_2O$) were purchased from Sigma-Aldrich. Aluminum isopropoxide (>98.0%) and sodium hydroxide beads (NaOH, 98.0%) were purchased from SAMCHUN. The deionized (DI) water used in all procedures and analytical measurements was purified with an aqua MAX Ultra 370 Series purification system (18.2 Ω) (YOUNGIN CHROMAS, Republic of Korea). All chemicals were used as received without further purification.

2.2. Synthesis of Silicalite-1 Nanocrystals

Silicalite-1 nanocrystals were synthesized using a two-stage varying-temperature synthesis procedure with a sol composition of 114 H_2O:2.49 TPAOH:0.8 NaOH:10 SiO_2. First, 8.93 g of a 1.0 M TPAOH solution was mixed with 0.16 g of DI water, following by the addition of 0.127 g of sodium hydroxide. After dissolution for 30 min, 2.5 g of silicic acid was added as the silica source to the reaction mixture. The mixture was vigorously stirred at 30 °C for 24 h and stored in a convection oven at 100 °C for 2 d, after reaction at 60 °C for 6 d. Then, the white precipitate in the reaction mixture was washed three times with DI water by centrifugation at 13,000 rpm. The resulting product was then redispersed in DI water by sonication.

2.3. Synthesis of Conventional Al-ZSM-5

Conventional micron-sized ZSM-5 crystals were synthesized using precursor sols with 4050 H_2O:4.5 TPAOH:20 SiO_2:x Al_2O_3:2x NaOH (where x = 0.29, 0.25, 0.15, 0.07, and 0). The mixture was stirred at 30 °C for 24 h. The precursor sol was filtered through a 0.45 μm (polypropylene) syringe filter, and the mixture was transferred into a Teflon-lined stainless-steel autoclave. Then, hydrothermal treatment was conducted at 150 °C for 3 d, and the product was washed with DI water by centrifugation at 13,000 rpm and redispersed in DI water.

2.4. Synthesis of Al-ZSM-5 Nanocrystals

Al-ZSM-5 crystals were synthesized using the seeded growth method with silicalite-1 nanocrystals as seeds. Typically, precursor sols with 4050 H_2O:4.5 TPAOH:20 SiO_2:x Al_2O_3:2x NaOH, (where x = 0.63, 0.29, 0.25, 0.14, 0.07, and 0) were stirred at 30 °C for 24 h. After the precursor sol was filtered with a 0.45 μm (polypropylene) syringe filter, a predetermined amount of silicalite-1 nanocrystals was added to the precursor sols. The mixture was transferred into a Teflon-lined stainless-steel autoclave, and hydrothermal synthesis was carried out. The synthesized crystals were calcined at 550 °C for 6 h at a ramp rate of 1 °C/min to remove the organic template.

2.5. Ion Exchange

The synthesized crystal samples were ion-exchanged in an aqueous NH_4NO_3 solution. Then, 1 g of zeolite was added to 25 mL of NH_4NO_3 solution (0.5 M), and the mixture was stored at 60 °C for 3 h and stirred. Following the ion-exchange process, samples were washed with DI water. This step was repeated three times, and the final samples were dried overnight at 60 °C. Dried samples were calcined at 500 °C for 3 h at a ramp rate of 1 °C/min.

2.6. Preparation of the Mo/HZSM-5 Catalysts

The Mo/HZSM-5 catalysts were prepared using a conventional wet impregnation method. The nano-seeded Al-ZSM-5 zeolites and commercial Al-ZSM-5 zeolites (SiO_2/Al_2O_3 = 5.75, 70, Zeolyst) were obtained via calcination of the NH_4-ZSM-5 zeolites at 500 °C for 5 h in air to convert NH_4^+ into H^+ prior to impregnation. Ammonium heptamolybdate ($(NH_4)_6Mo_7O_{24}\cdot4H_2O$, Sigma-Aldrich) was used as the Mo precursor; the Mo content in

the catalysts was 4 wt% (4Mo/HZSM-5). Following impregnation with Mo, the impregnated powder was dried at 80 °C for 12 h, followed by calcination at 500 °C for 5 h in air. Catalysts were pressed to form pellets; these were crushed and sieved to obtain a particle size of 212–500 μm (35–70 mesh) for use in the catalytic reactions.

2.7. MDA Reaction

The MDA reactions were conducted using 0.3 g of the catalysts in a fixed bed, and a tubular quartz reactor (inner diameter of 10 mm) at atmospheric pressure and 700 °C. The reactor effluent was transferred via heated transfer lines to a gas chromatograph (GC; Agilent 7890). The methane conversion was calculated on a carbon atom basis based on all carbon-containing products using Equation (1):

$$\%S_i = \frac{n_i}{\sum_i n_i} \tag{1}$$

where *i* is the carbon-containing species and *n* is the number of carbon atoms in species *i*.

2.8. Characterization

The XRD patterns of samples were recorded using a New DB-Advance (CuKα radiation) diffractometer (Bruker-AXS, USA). The product FE-SEM images and EDS mapping images were obtained by SIGMA (Carl Zeiss, Germany). The N_2 adsorption and desorption isotherms of all samples were obtained using an ASAP 2020 system (Micromeritics, USA).

3. Results and Discussion

The diffusion channel lengths of the Al-ZSM-5 catalyst affects catalyst stability and product selectivity in the MDA reaction [11,12]. Based on previous research, we attempted to prepare Al-ZSM-5 catalysts with sub-100 nm diffusion channels to evaluate the impacts of nanoscopic change in diffusion channels on catalyst stability. To do this, monodisperse Al-ZSM-5 nanocrystals exhibiting similar diffusion channels that were <100 nm were required. It was important that these crystals had a sufficiently high crystallinity to function as an acid catalyst for the MDA reaction. Figure 1 shows SEM imagery of Al-ZSM-5 crystals prepared under varying SARs at 150 °C for 3 d without the addition of seed crystals. It may be possible to prepare an Al-ZSM-5 crystal that was <100 nm by lowering the synthesis temperature or by using a highly concentrated sol composition. As these methods often result in low-crystalline zeolite crystals [31], this study investigated the conventional Al-ZSM-5 sol recipes and synthesis conditions. Figure 1 shows that with decreasing SAR, the crystal size of the zeolite decreases, whereby the external surface of the zeolite becomes rough. Zeolite synthesized without Al in sol (see Figure 1a) had the largest crystal size of >3 μm. The sol condition of SAR 35 produced the smallest Al-ZSM-5 size, <1 μm, (see Figure 1e). Additionally, Al-ZSM-5 was not synthesized under conditions where the SAR was <30. Figure 1 shows that all zeolite crystals were micron in size, and particle size was broadly distributed at every synthesis condition.

Figure 2 shows zeolite synthesized in the presence of silicalite-1 seeds. The presence of seeds in zeolite synthesis sols critically altered crystallization mechanics, impacting upon crystallization time, crystal size, and zeolites morphology [33]. The seed crystals in the synthesis sols became the zeolite growth core, nuclei provider, and nucleation promoters depending on their size and composition [32]. The silicalite-1 seed crystal (30–40 nm) in Figure 2a was used to prepare Al-ZSM-5 crystals. The solubility of silica in the synthesis sols had significantly been altered with the addition of the aluminum source [36], where the silicalite-1 seeds seemingly dissolved in the aluminosilicate sol. However, Figure 2b–g demonstrates that the silicalite-1 seeds grew larger than the seed crystal. This indicates that silicalite-1 did not dissolve in the aluminosilicate sol and served as seeds for Al-ZSM-5 growth. Figure 2 shows that zeolites with different SARs had significantly different crystal sizes and morphologies. For the zeolite (SAR = ∞) in Figure 2b, crystal size increased to 300 nm, and a smooth external surface was observed. In comparison to Figure 1a, where

it had been synthesized without a seed crystal, there was a 10-fold decrease in crystal size. With a decrease in the SAR ratio, the crystal size decreased and the external surface gradually became rough and bumpy, as shown in Figure 2b–f. Further decreases in the SAR to 25 produced a crystal that was the same size as that of silicalite-1, shown in Figure 2g; the crystal yield in the synthesis was negligible in this case. It is known that low SARs promote the nucleation of zeolites, resulting in a decrease in crystal size [37]. However, the observed decrease in crystal size may be associated with a different factor as crystal growth occurred on the surface of the silicalite-1 seeds, as shown in Figure 2. Table 1 provides the weights of the prepared zeolite crystals and the number of crystals in each batch. The calculation method and assumption are given in the supporting materials. The possible error is 15%; thus, data presented in Table 1 are roughly approximated. This table shows that with a decrease in SAR, the weight of zeolite products had reduced with the number of crystals. Thus, low SARs did not stimulate zeolite nucleation. However, the change in silica solubility following the addition of aluminum species is considered to have contributed to the decrease in the crystal size. As such, the increase in the solubility of sols with the addition of aluminum species decreased the nutrient supersaturation, and eventually reduced the driving force for zeolite growth, resulting in a decrease in crystal size.

Table 1. Weight and number of particles of the zeolites with different SARs *.

Catalyst (Si/Al Ratio)	Weight of Formed Zeolite (g)	Average Particle Size (nm)	Particle Volume (nm^3)	Number of Particles (Counts)
∞	0.21	250	6,750,000	1.75×10^{13}
140	0.13	230	4,264,000	1.71×10^{13}
70	0.08	200	3,141,593	1.43×10^{13}
40	0.05	180	3,053,628	9.17×10^{12}
35	0.027	150	1,767,146	8.57×10^{12}
25	0.001	80	268,083	6.76×10^{12}

* Calculations for weight, average particle size, particle volume, and number of zeolite particles are described in the Supporting Information.
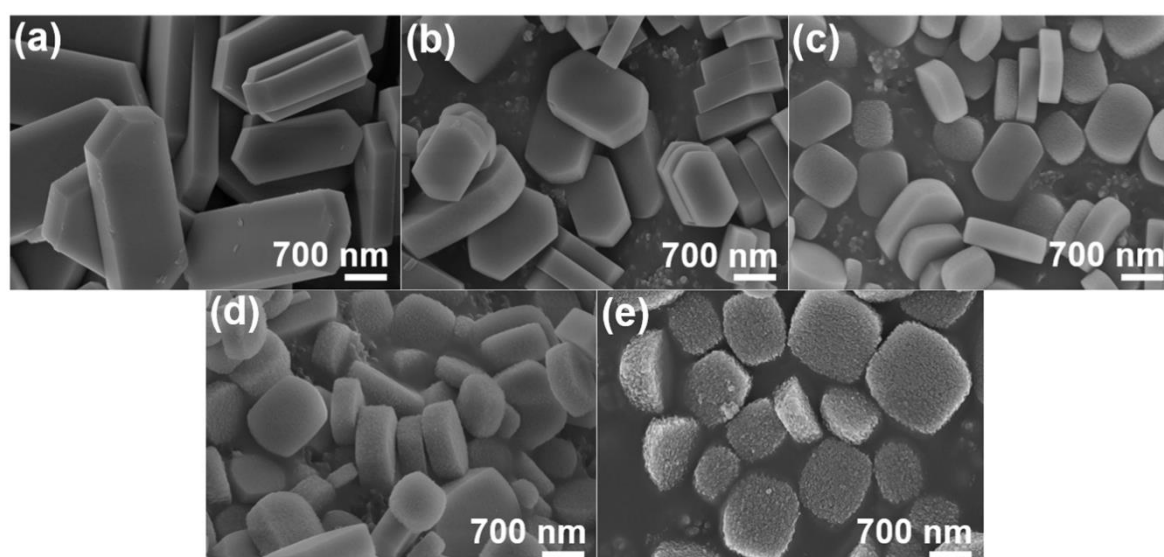

Figure 1. Zeolite growth without silicalite-1 seed crystals. SEM imagery of the Al-ZSM-5 crystal samples with (**a**) SAR = ∞; (**b**) SAR = 140; (**c**) SAR = 70; (**d**) SAR = 40; and (**e**) SAR = 35. The synthesis was conducted at 150 °C for 3 d under different sol compositions: 4050 H$_2$O:4.5 TPAOH:20 SiO$_2$:x Al$_2$O$_3$:2x NaOH, where x was dependent on the SAR.
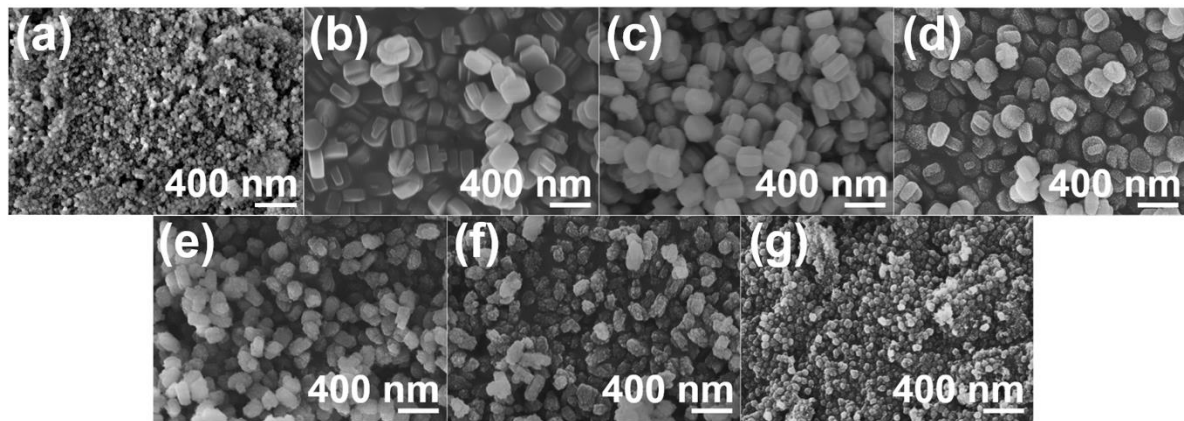
Figure 2. Zeolite synthesized in the presence of silicalite-1 seed. SEM imagery of (**a**) silicalite-1 seed crystals; and (**b**–**g**) seeded grown Al-ZSM-5 zeolites with different SARs. SEM imagery of the zeolites synthesized with sol compositions of (**b**) SAR = ∞; (**c**) SAR = 140; (**d**) SAR = 70; (**e**) SAR = 40; (**f**) SAR = 35; and (**g**) SAR = 25. The sol composition was 4050 H_2O:4.5 TPAOH:20 SiO_2:x Al_2O_3:2x NaOH, where x = 0, 0.07, 0.15, 0.25, 0.29, and 0.63, following the addition of silicalite-1 seeds (3.62×10^{-2} wt%: the weight ratio of silicalite-1 nanocrystals and TEOS). The synthesis was conducted at 150 °C for 24 h.

Once a basic understanding of the preparation of Al-ZSM-5 using the seeded growth approach was obtained, we attempted to decrease the Al-ZSM-5 crystal size to 100 nm. Figure 3 shows the crystal size change of Al-ZSM-5 based on reaction time at 120 °C. Figure 3a shows that following synthesis for 1 h, there was aggregative growth of the Al-ZSM-5 crystal on the surface of silicalite-1, where morphologies became irregular and rough. The typical coffin shape of ZSM-5 was observed, and twinning of the crystals occurred after 2 h of crystallization (Figure 3c). The zeolites grew continuously for up to 4 h (Figure 3d–e). Once a crystal size of 230 nm was achieved (Figure 3f), further crystal growth was not observed by SEM. As shown in Figure 3g of crystal growth according to synthesis time, crystal growth was rapid during the early stages of growth, and crystal size was similar in size to the zeolite crystallized after 5 h under the same conditions. Thus, Al-ZSM-5 crystals that were <100 nm in size could be prepared upon crystal growth for less than 2 h.
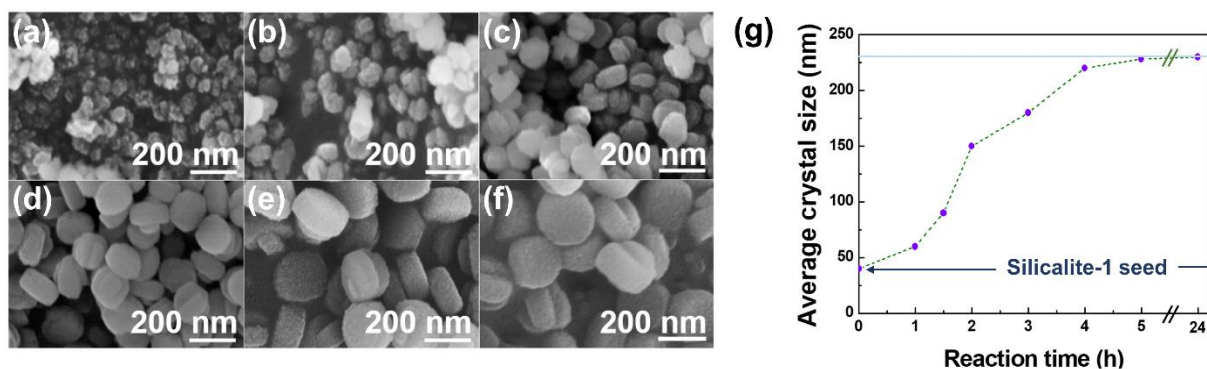

Figure 3. Crystal size change of Al-ZSM-5 based on reaction time. SEM imagery of seeded grown Al-ZSM-5 after crystallization at 120 °C for (**a**) 1 h; (**b**) 1.5 h; (**c**) 2 h; (**d**) 3 h; (**e**) 4 h; and (**f**) 5 h. Zeolite growth was conducted using the synthesis sols of 4050 H_2O:4.5 TPAOH:20 SiO_2:x Al_2O_3:2x NaOH (x = 0.07). The amount of the silicalite-1 seeds relative to TEOS, was 3.62×10^{-2} wt%. (**g**) Changes in crystal size according to reaction time. The average particle size of silicalite-1 seeds and maximum crystal size are marked in the dark blue line and bright blue line, respectively.

Controlling the relative concentrations of zeolite seeds and a silica/alumina nutrient has been reported as an efficient approach to refine the size of synthesized crystals [37,38]. As such, we also tuned the relative concentrations of silicalite-1 seeds and the SARs (Figure 4). The size of Al-ZSM-5 had a clear dependence on the relative concentrations of

the silicalite-1 seeds and nutrients (silica/alumina). Figure 4a–c show that the crystal size had gradually increased from 100 to 800 nm with a decrease in the silicalite-1 concentration relative to the TEOS as the silica nutrient in the sol with a SAR of 140. This indicates that most of the silica/alumina nutrient in the synthesis sol was consumed for crystal growth as opposed to creating another homogeneous nucleation. The sol with an SAR of 35 exhibited a similar trend as that shown by the sol with an SAR of 140. However, the crystal size for the former was smaller (80–600 nm) than the latter; this may be attributed to the solubility change discussed previously. The crystal size decrease based on silicalite-1 seeds relative to TEOS is depicted in Figure 4g, where Al-ZSM-5 was prepared using the silicalite-1 seeds relative to TEOS of >0.18. Compared with the approach to control crystal size by reaction time, this method may provide a sufficient amount of crystallization time for the evolution of Al-ZSM-5 and reduce the costs associated with expensive chemicals. Thus, Al-ZSM-5 nanocrystals with different SARs for the MDA reaction were prepared by tuning the relative ratio of silicalite-1 seeds and silica/alumina nutrients.
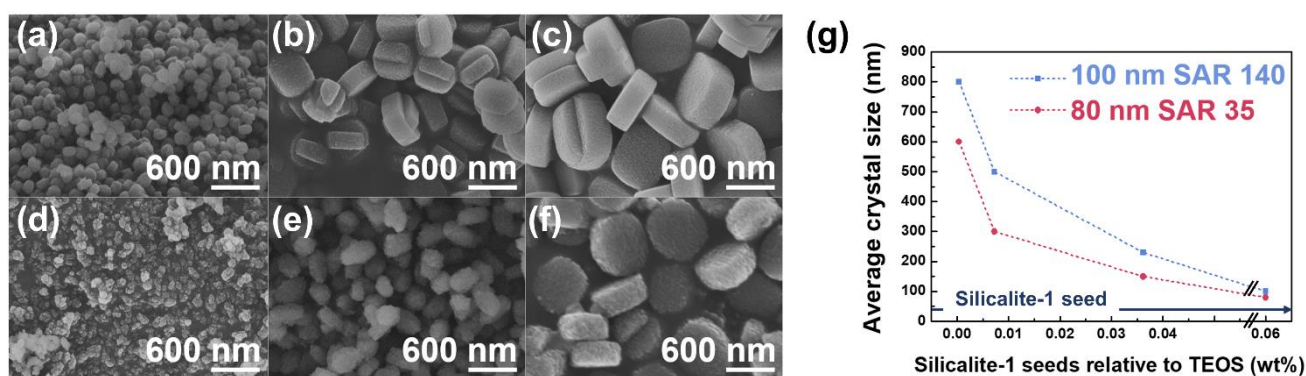

Figure 4. Changes in the crystal size of the samples depending on the relative amounts of the silicalite-1 seed and Si/Al nutrients. SEM imagery of the zeolite samples with (**a**–**c**) SAR = 140; and (**d**–**f**) SAR = 35. The precursor sol composition was 4050 H_2O:4.5 TPAOH:20 SiO_2:x Al_2O_3:2x NaOH, where the values of x were 0.07 and 0.29, while the relative amount of silicalite-1 seeds was 0.18 wt% for (**a**,**d**), 7.24×10^{-3} for (**b**,**e**) and 3.62×10^{-4} wt% for (**c**,**f**). Growth was conducted at 150 °C for 48 h; (**g**) changes in crystal size according to relative ratio of silicalite-1 seeds and silica/alumina nutrients. The average particle size of silicalite-1 seeds is marked by the dark blue line.

Two Al-ZSM-5 crystals with SARs of 35 and 140 were prepared for the MDA reaction. Samples were labeled as 80 nm SAR 35 and 100 nm SAR 140; the first number denotes the crystal size, while the second denotes the SAR of the synthesis sol used for crystallization of the zeolite samples. Figure 5 shows the SEM, EDS, XRD, and N_2 isotherm profiles of the zeolite samples. Figure 5a shows that the 100 nm SAR 140 sample exhibited a slightly coarsened surface and had adopted an irregular elliptical shape, the latter being similar to that of the silicalite-1 crystal. The distribution of Al in this sample was observed using EDS mapping; the intensity was weak, possibly due to its small crystal size and low Al content. The 80 nm SAR 35 sample also possessed an irregular crystal shape with spherical protrusions, exhibiting aggregative growth. The Al distribution on the crystal may be detected by EDS, although the intensity was not strong, similar to that of 100 nm SAR 140. As observed from the XRD pattern (Figure 5c), two samples showed a pure MFI structure. The N_2 isotherm measurements were conducted on the Al-ZSM-5 samples prior to and after Mo species loading, where this loading into the micropores of Al-ZSM-5 is a necessary step for the MDA reaction [39]. Al-The results from the samples are shown in Figure 4f and Table 2. A clear uptake of N_2 was observed in the low relative pressure region ($P/P_0 < 0.01$) for all samples, indicating the presence of micropores in the samples. There was large N_2 adsorption in the high-pressure region ($P/P_0 > 0.9$), due to void gaps of small particle aggregations. The micropore volumes of the 100 nm SAR 140 and 80 nm SAR 35 were 0.15 mL/g and 0.13 mL/g, respectively. This was determined using the t-plot method (Table 2). As such, these samples exhibited a highly crystalline structure. After loading

the Mo species for the MDA reaction, although there were clear reductions in the external surface areas, there were only small changes in the micropore areas (BET area-external surface area) responsible for methane conversion. Thus, Mo species were loaded on the micropores of zeolite without severe blockage of pores.
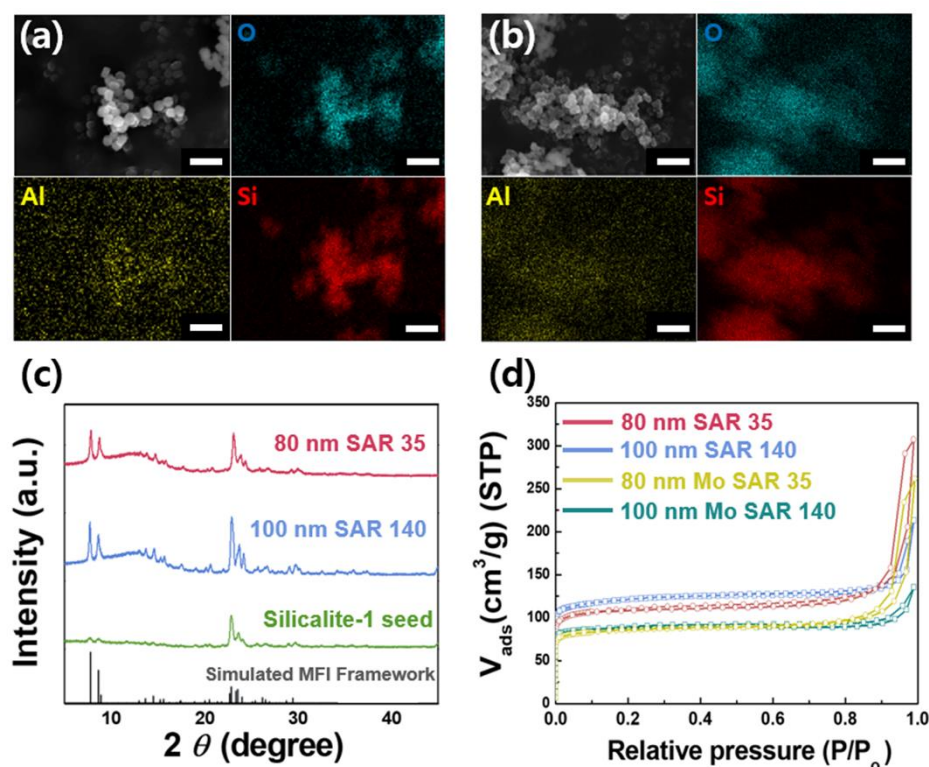

Figure 5. Morphologies and texture properties of seeded grown ZSM-5 with different sizes and SARs. EDS results for (**a**) 100 nm SAR 140; and (**b**) 80 nm SAR 35. Si, O, and Al are marked in red, sky blue, and yellow, respectively; (**c**) powder XRD patterns; and (**d**) N_2 isotherms of samples. The white horizontal scale bar represents 500 nm.

Table 2. Texture properties of the seeded grown Al-ZSM-5 zeolite samples.

Catalyst	V_{total} [a] (cm^3/g)	V_{micro} [b] (cm^3/g)	S_{BET} [c] (m^2/g)	S_{ext} [d] (m^2/g)
80 nm SAR 35	0.23	0.13	432	92
80 nm Mo SAR 35	0.18	0.11	336	59
100 nm SAR 140	0.22	0.15	473	92
100 nm Mo SAR 140	0.15	0.12	335	14

[a] Total pore volume taken from the volume of N_2 adsorbed at $P/P_0 = 0.99$. [b] Micro pore volume calculated from t-plot. [c] BET surface area. [d] External surface area.

The MDA reaction was then conducted using Mo-impregnated Al-ZSM-5 nanocrystal samples. Figure 6 shows the methane conversion efficiency of zeolites as a function of the time-on-stream (TOS) at atmospheric pressure and at 700 °C. Commercial Al-ZSM-5 crystals with SARs of 140 and 11.5 were also tested for a parallel comparison. The aromatic selectivities obtained using 100 nm SAR 140 and commercial zeolite with SAR 140 are also given in Figure S1 (Supplementary Material). Since SAR of synthesized catalysts and commercial ones were not the same, only qualitative comparison was viable. Following 1 h of induction, the conversion in the presence of each zeolite sample had reached 12% of the equilibrium conversion for all samples, and gradually decreased because of catalyst deactivation. The 80 nm Mo SAR 35 and 100 nm Mo SAR 140 samples had slightly higher methane conversion than commercial zeolite samples at early TOS from 1 to 3 h.

However, there was only a marginal difference, whereby clear deactivation trends were also observed. There was no clear difference in the SAR of both Al-ZSM-5 nanocrystals and commercial Al-ZSM-5 crystals. Although the Al-ZSM-5 nanocrystals prepared in this study functioned as catalysts for the MDA reaction, there was no significant improvement in methane conversion efficiency and catalyst deactivation compared to conventional zeolite samples. This indicates that further research is needed to develop catalysts that satisfy these requirements for commercialization. In future, the preparation of Al-ZSM-5 crystals with various diffusional channels, and MDA reaction performance evaluation in terms of catalyst stability and product selectivity is important.
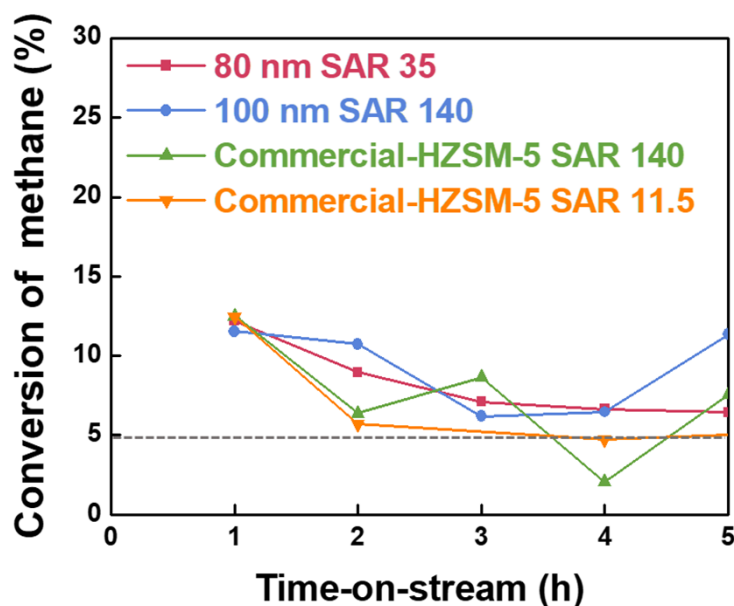

Figure 6. Methane conversion efficiency of seeded grown Al-ZSM-5 as a function of the TOS obtained from obtained from gas chromatograph (GC) analysis. The gray dotted lines indicate the methane conversion line of 5%.

4. Conclusions

This study evaluated the catalyst stability of Al-ZSM-5 nanocrystals that were grown on silicalite-1 seeds, during the MDA reaction. The SAR of the synthesis sol impacted the crystal size and surface morphology of the samples. Samples with low SARs were small, rough crystals. It was observed that the size of the Al-ZSM-5 crystals could be controlled by the synthesis time and the amount of silicalite-1 seeds relative to the Si/Al nutrients, while the latter was more effective in obtaining monodisperse nanocrystalline Al-ZSM-5. Two Al-ZSM-5 nanocrystals that were <100 nm with different SARs were prepared and used for the MDA reaction. Methane conversion was up to 12% of the thermodynamic equilibrium conversion at 700 °C in both samples. The conversion gradually decreased because of deactivation. Compared with commercial zeolite, synthesized Al-ZSM-5 nanocrystals demonstrated improved stability in the MDA reaction, albeit with small changes. However, the SAR of the catalyst exhibited no noticeable changes in catalyst stability. This indicates that the diffusion channel length of the catalyst in the nanoscopic range is an effective factor influencing catalyst stability, while the improvement is not sufficient for commercialization. As such, other catalyst properties and reaction engineering should be combined to obtain a commercial-scale MDA catalyst; future research in this direction is necessary.

Supplementary Materials: The following are available online at https://www.mdpi.com/1996-1073/14/2/485/s1, Method of zeolite size and number density calculation.

References

1. Čejka, J.; Centi, G.; Perez-Pariente, J.; Roth, W.J. Zeolite-based materials for novel catalytic applications: Opportunities, perspectives and open problems. *Catal. Today* **2012**, *179*, 2–15. [CrossRef]
2. Fechete, I.; Wang, Y.; Védrine, J.C. The past, present and future of heterogeneous catalysis. *Catal. Today* **2012**, *189*, 2–27. [CrossRef]
3. Schwach, P.; Pan, X.; Bao, X. Direct Conversion of Methane to Value-Added Chemicals over Heterogeneous Catalysts: Challenges and Prospects. *Chem. Rev.* **2017**, *117*, 8497–8520. [CrossRef] [PubMed]
4. Sun, K.; Ginosar, D.M.; He, T.; Zhang, Y.; Fan, M.; Chen, R. Progress in Nonoxidative Dehydroaromatization of Methane in the Last 6 Years. *Ind. Eng. Chem. Res.* **2018**, *57*, 1768–1789. [CrossRef]
5. Xu, Y.; Chen, M.; Wang, T.; Liu, B.; Jiang, F.; Liu, X. Probing cobalt localization on HZSM-5 for efficient methane dehydroaromatization catalysts. *J. Catal.* **2020**, *387*, 102–118. [CrossRef]
6. Xu, Y.; Chen, M.; Liu, B.; Jiang, F.; Liu, X. CH4 conversion over Ni/HZSM-5 catalyst in the absence of oxygen: Decomposition or dehydroaromatization? *Chem. Commun.* **2020**, *56*, 4396–4399. [CrossRef] [PubMed]
7. Vollmer, I.; Ould-Chikh, S.; Aguilar-Tapia, A.; Li, G.; Pidko, E.A.; Hazemann, J.-L.; Kapteijn, F.; Gascon, J. Activity Descriptors Derived from Comparison of Mo and Fe as Active Metal for Methane Conversion to Aromatics. *J. Am. Chem. Soc.* **2019**, *141*, 18814–18824. [CrossRef]
8. Lim, T.H.; Kim, D.H. Characteristics of Mn/H-ZSM-5 catalysts for methane dehydroaromatization. *Appl. Catal. A Gen.* **2019**, *577*, 10–19. [CrossRef]
9. Wang, K.; Huang, X.; Li, D. Hollow ZSM-5 zeolite grass ball catalyst in methane dehydroaromatization: One-step synthesis and the exceptional catalytic performance. *Appl. Catal. A Gen.* **2018**, *556*, 10–19. [CrossRef]
10. Zhu, P.; Yang, G.; Sun, J.; Fan, R.; Zhang, P.; Yoneyama, Y.; Tsubaki, N. A hollow Mo/HZSM-5 zeolite capsule catalyst: Preparation and enhanced catalytic properties in methane dehydroaromatization. *J. Mater. Chem. A* **2017**, *5*, 8599–8607. [CrossRef]
11. Wu, Y.; Emdadi, L.; Wang, Z.; Fan, W.; Liu, D. Textural and catalytic properties of Mo loaded hierarchical meso-/microporous lamellar MFI and MWW zeolites for direct methane conversion. *Appl. Catal. A Gen.* **2014**, *470*, 344–354. [CrossRef]
12. Liu, Y.; Zhao, M.; Cheng, L.; Yang, J.; Liu, L.; Wang, J.; Yin, D.; Lu, J.; Zhang, Y. Facile synthesis and its high catalytic performance of hierarchical ZSM-5 zeolite from economical bulk silicon oxides. *Microporous Mesoporous Mater.* **2018**, *260*, 116–124. [CrossRef]
13. Kosinov, N.; Hensen, E.J. Reactivity, Selectivity, and Stability of Zeolite-Based Catalysts for Methane Dehydroaromatization. *Adv. Mater.* **2020**, *32*, e2002565. [CrossRef] [PubMed]
14. Xu, Y.; Song, Y.; Zhang, Z. A binder-free fluidizable Mo/HZSM-5 catalyst for non-oxidative methane dehydroaromatization in a dual circulating fluidized bed reactor system. *Catal. Today* **2017**, *279*, 115–123. [CrossRef]
15. Morejudo, S.H.; Zanón, R.; Escolástico, S.; Yuste-Tirados, I.; Malerød-Fjeld, H.; Vestre, P.K.; Coors, W.G.; Martínez, A.; Norby, T.; Serra, J.M.; et al. Direct conversion of methane to aromatics in a catalytic co-ionic membrane reactor. *Science* **2016**, *353*, 563–566. [CrossRef] [PubMed]
16. Jeong, J.; Hwang, A.; Kim, Y.T.; Hong, D.-Y.; Park, M.-J. Kinetic modeling of methane dehydroaromatization over a Mo2C/H-ZSM5 catalyst: Different deactivation behaviors of the Mo2C and H-ZSM5 sites. *Catal. Today* **2020**, *352*, 140–147. [CrossRef]
17. Zhang, T.; Yang, X.; Ge, Q. CH4 dissociation and C C coupling on Mo-terminated MoC surfaces: A DFT study. *Catal. Today* **2020**, *339*, 54–61. [CrossRef]
18. Ha, V. Aromatization of methane over zeolite supported molybdenum: Active sites and reaction mechanism. *J. Mol. Catal. A Chem.* **2002**, *181*, 283–290. [CrossRef]
19. Liu, L.; Wang, N.; Zhu, C.; Liu, X.; Zhu, Y.; Guo, P.; Alfilfil, L.; Dong, X.; Zhang, D.; Han, Y. Direct Imaging of Atomically Dispersed Molybdenum that Enables Location of Aluminum in the Framework of Zeolite ZSM-5. *Angew. Chem.* **2019**, *132*, 829–835. [CrossRef]

20. Kosinov, N.; Coumans, F.J.A.G.; Uslamin, E.A.; Wijpkema, A.S.G.; Mezari, B.B.; Hensen, E.J. Methane Dehydroaromatization by Mo/HZSM-5: Mono- or Bifunctional Catalysis? *ACS Catal.* **2017**, *7*, 520–529. [CrossRef]

21. Choi, M.; Na, K.; Kim, J.; Sakamoto, Y.; Terasaki, O.; Ryoo, R. Stable single-unit-cell nanosheets of zeolite MFI as active and long-lived catalysts. *Nat. Cell Biol.* **2009**, *461*, 246–249. [CrossRef]

22. Jeon, M.Y.; Kim, D.; Kumar, P.; Lee, P.S.; Rangnekar, N.; Bai, P.; Shete, M.; Elyassi, B.; Lee, H.-S.; Narasimharao, K.; et al. Ultra-selective high-flux membranes from directly synthesized zeolite nanosheets. *Nat. Cell Biol.* **2017**, *543*, 690–694. [CrossRef]

23. Na, K.; Park, W.; Seo, Y.; Ryoo, R. Disordered Assembly of MFI Zeolite Nanosheets with a Large Volume of Intersheet Mesopores. *Chem. Mater.* **2011**, *23*, 1273–1279. [CrossRef]

24. Zhang, X.; Liu, D.; Tsapatsis, M.; Asahina, S.; Cychosz, K.A.; Agrawal, K.V.; Al Wahedi, Y.; Bhan, A.; Al Hashimi, S.; Terasaki, O.; et al. Synthesis of Self-Pillared Zeolite Nanosheets by Repetitive Branching. *Science* **2012**, *336*, 1684–1687. [CrossRef]

25. Cho, H.S.; Ryoo, R. Synthesis of ordered mesoporous MFI zeolite using CMK carbon templates. *Microporous Mesoporous Mater.* **2012**, *151*, 107–112. [CrossRef]

26. Ma, Q.; Fu, T.; Wang, Y.; Li, H.; Cui, L.; Li, Z. Development of mesoporous ZSM-5 zeolite with microporosity preservation through induced desilication. *J. Mater. Sci.* **2020**, *55*, 11870–11890. [CrossRef]

27. Ma, Q.; Fu, T.; Li, H.; Cui, L.; Li, Z. Insight into the Selection of the Post-Treatment Strategy for ZSM-5 Zeolites for the Improvement of Catalytic Stability in the Conversion of Methanol to Hydrocarbons. *Ind. Eng. Chem. Res.* **2020**, *59*, 11125–11138. [CrossRef]

28. Kim, S.; Park, G.; Woo, M.H.; Kwak, G.; Kim, S.K. Control of Hierarchical Structure and Framework-Al Distribution of ZSM-5 via Adjusting Crystallization Temperature and Their Effects on Methanol Conversion. *ACS Catal.* **2019**, *9*, 2880–2892. [CrossRef]

29. Wang, J.; Zhang, R.; Han, L.; Wang, J.; Zhao, L. Seed-assisted synthesis and characterization of nano and micron ZSM-5 molecular sieves in template-free system. *J. Solid State Chem.* **2020**, *290*, 121536. [CrossRef]

30. Zhang, C.; Wu, Q.; Lei, C.; Han, S.; Zhu, Q.; Maurer, S.; Dai, D.; Parvulescu, A.-N.; Mueller, U.; Meng, X.; et al. An efficient, rapid, and non-centrifugation synthesis of nanosized zeolites by accelerating the nucleation rate. *J. Mater. Chem. A* **2018**, *6*, 21156–21161. [CrossRef]

31. Li, T.; Krumeich, F.; Van Bokhoven, J.A. Where Does the Zeolite ZSM-5 Nucleation and Growth Start? The Effect of Aluminum. *Cryst. Growth Des.* **2019**, *19*, 2548–2551. [CrossRef]

32. Nada, M.H.; Larsen, S.C. Insight into seed-assisted template free synthesis of ZSM-5 zeolites. *Microporous Mesoporous Mater.* **2017**, *239*, 444–452. [CrossRef]

33. Javdani, A.; Ahmadpour, J.; Yaripour, F. Nano-sized ZSM-5 zeolite synthesized via seeding technique for methanol conversions: A review. *Microporous Mesoporous Mater.* **2019**, *284*, 443–458. [CrossRef]

34. Xue, T.; Chen, L.; Wang, Y.M.; He, M.-Y. Seed-induced synthesis of mesoporous ZSM-5 aggregates using tetrapropylammonium hydroxide as single template. *Microporous Mesoporous Mater.* **2012**, *156*, 97–105. [CrossRef]

35. Chen, L.; Xue, T.; Wu, H.; Wu, P. Hierarchical ZSM-5 nanocrystal aggregates: Seed-induced green synthesis and its application in alkylation of phenol with tert-butanol. *RSC Adv.* **2018**, *8*, 2751–2758. [CrossRef]

36. Cundy, C.S.; Cox, P.A. The Hydrothermal Synthesis of Zeolites: Precursors, Intermediates and Reaction Mechanism. *Microporous Mesoporous Mater.* **2005**, *36*, 1–78. [CrossRef]

37. Ren, X.-Y.; Cao, J.-P.; Zhao, X.-Y.; Yang, Z.; Wang, Y.-J.; Chen, Q.; Zhao, M.; Wei, X.-Y. Catalytic conversion of lignite pyrolysis volatiles to light aromatics over ZSM-5: SiO_2/Al_2O_3 ratio effects and mechanism insights. *J. Anal. Appl. Pyrolysis* **2019**, *139*, 22–30. [CrossRef]

38. Ghorbanpour, A.; Gumidyala, A.; Grabow, L.C.; Crossley, S.; Rimer, J.D. Epitaxial Growth of ZSM-5@Silicalite-1: A Core–Shell Zeolite Designed with Passivated Surface Acidity. *ACS Nano* **2015**, *9*, 4006–4016. [CrossRef]

39. Gao, J.; Zheng, Y.; Jehng, J.-M.; Tang, Y.; Wachs, I.E.; Podkolzin, S.G. Identification of molybdenum oxide nanostructures on zeolites for natural gas conversion. *Science* **2015**, *348*, 686–690. [CrossRef]